Journal of Engineering Mechanics and Machinery (2024)
Clausius Scientific Press, Canada

DOI: 10.23977/jemm.2024.090207
ISSN 2371-9133 Vol. 9 Num. 2

Flow field simulation and structural optimization of the top fan drying room based on CFD

Yifeng Zhu[1,a,*], Liping Sun[1,b], Jiuqiang Wang[2,c]

[1]Northeast Forestry University, Harbin, 150040, China
[2]Harbin Engineering University, Harbin, 150040, China
[a]zhuyifeng@nefu.edu.cn, [b]zdhslp@163.com, [c]wangjiuqiang@hrbeu.edu.cn
[*]Corresponding author

Keywords: Drying room; numerical simulation; structural optimization; airflow distribution; wind-speed uniformity

Abstract: In order to improve the wind-speed uniformity field distribution in the hot air drying room, the numerical simulation analysis of the internal three-dimensional wind speed field was carried out by using the hot air drying room of the top fan type as the model. The wind-speed uniformity field was used to quantify the evaluation index, and the optimal scheme was screened by data comparison analysis. Eight structural optimization schemes were proposed by using three design methods: curved right-angle structure, adjustment of saw spacing, and increase or decrease of the number of average wind plates. The wind speed field distribution between the original structure model and the Structure optimization scheme under different wind speeds was compared (3m/s, 5m/s, 7m/s) and analyzed. It was found that there was a positive correlation between the wind speed data between the air inlet and the sampling point. The test results show that when the inlet wind speed is 5m/s, the velocity non-uniformity coefficient of optimal scheme B2 is 82.34% lower than that of the original structure model, the difference of wind speed sampling points is reduced by 106.2%, and the average wind speed in the drying room is increased by 12.88%. After the structural optimization, the area of the low-speed turbulent region of the drying room is reduced, the wind speed difference in the drying area is reduced, and the wind-speed uniformity in the drying room is improved.

1. Introduction

Hot air drying is a widely used drying method in industrial and agricultural production [1]. Sawn timber drying is an important part of wood processing and production [2]. To achieve efficient and green drying of sawn timber is one of the hotspots in the field of hot air drying [3]. The hot air drying room of the top fan type is a typical mechanical device in the sawn timber drying process [4]. The uneven distribution of the internal wind speed field is the main factor affecting the drying quality and efficiency of the sawn timber [5].

Coban et al [6] used CFD (Computational Fluid Dynamics) software to simulate and predict the flow field movement of drying process in complex scenes in different physical environments. Kadem et al. [7] developed a three-dimensional comprehensive model of sawn timber drying and

carried out finite element analysis. Chen et al. [8] optimized the structure of the inlet variable diameter angular tube, and verified the effectiveness of the optimization scheme to solve the problem of uneven airflow distribution in the dryer by using FLUENT software. Based on the numerical simulation results of airflow distribution in the drying room, Wang et al. [9] realized the problem of unstable product quality and low drying efficiency in the drying process of the drying room by optimizing the structure and wind speed parameters of the drying room. Huo et al. [10] compared the measured value with the simulated value and determined that the error between the two was within 10%, so the simulation results of the wind speed field in the drying room were feasible. Although domestic and foreign scholars have made some achievements in the numerical simulation analysis of various types of drying rooms, the research on the wind speed field inside the drying room is mostly based on qualitative analysis [11], failing to combine the relevant quantitative evaluation indicators to analyze the uniformity of the wind speed field, and paying more attention to the structural optimization design of the drying room, while ignoring the research on the distribution law of the wind speed field inside the drying room and the data relationship between the wind speed data.

In this paper, the hot air drying room of the top fan type is used as the model, and the wind speed sampling point data is calculated and solved by the calculation formula for quantitative evaluation and qualitative analysis. The feasibility of the numerical simulation results is verified by experiments. Aiming at the problem of uneven distribution of wind field inside the hot air drying room, the structural optimization scheme of the drying room is proposed, and the superiority of the proposed scheme is verified by data comparison analysis and empirical analysis.

2. Numerical calculation model

2.1. Building the original structure model

The measured three-dimensional size data of the hot air drying room of the top fan type is 2100mm × 1400mm × 1500mm (length × width × height). The 3D structure model of the drying room under no-load condition is established by using SPACECLAIM software, as shown in Figure 1a. In order to reduce the consumption of computing resources, a three-dimensional simplified model of drying room and sawn timber under loading conditions is further established (here the wind speed field fluid domain of the axial flow fan in the ceiling partition is simplified). In order to improve the comprehensibility of the model, the wind speed field velocity distribution map of the key section of the simplified model (shown in Figure 1b) will be established at 1050 mm in the X-axis direction [12].

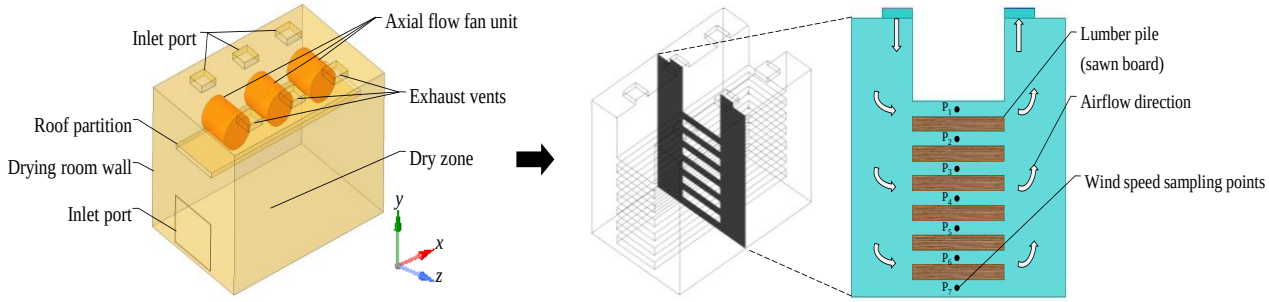

Figure 1: Original structural model

2.2. Numerical simulation

2.2.1. Turbulence model

The flow control equations used to establish the mathematical model of hot air drying room include continuity equation, momentum equation and Standard k-ε turbulent kinetic energy transport and dissipation equation [13-17], which are as follows:

The continuity equation and the momentum equation are:

$$\frac{\partial u_i}{\partial x_i} = 0 \tag{1}$$

$$\frac{\partial(\rho u_i u_j)}{\partial x_j} = -\frac{\partial P}{\partial x_j} + \frac{\partial}{\partial x_j}\left[\mu\left(\frac{\partial u_i}{\partial x_j} + \frac{\partial u_j}{\partial x_i}\right)\right] - \frac{2}{3}\frac{\partial}{\partial x_j} + \left(\mu\frac{\partial u_i}{\partial x_j}\right) + \rho g_i \tag{2}$$

In equations (1)-(2): μ is the dynamic viscosity; P is the air static pressure; x_i is the component of displacement in the i direction; x_j is the component of displacement in the j direction; u is the air flow velocity; $\rho$is the air density; g is the gravitational acceleration.

Standard k-εThe turbulent kinetic energy and dissipation rate transport equation of the model:

$$\frac{\partial(\rho k)}{\partial t} + \frac{\partial(\rho k u_i)}{\partial x_i} = \frac{\partial}{\partial x_j}\left[\left(\mu + \frac{\mu_i}{\sigma_k}\right)\frac{\partial k}{\partial x_j}\right] + G_k + G_b - \rho\varepsilon - Y_M + S_k \tag{3}$$

$$\frac{\partial(\rho\varepsilon)}{\partial t} + \frac{\partial(\rho\varepsilon u_i)}{\partial x_i} = \frac{\partial}{\partial x_j}\left[\left(\mu + \frac{\mu_i}{\sigma_\varepsilon}\right)\frac{\partial \varepsilon}{\partial x_j}\right] + C_{1\varepsilon}\frac{\varepsilon}{k}\left(G_k + C_{3\varepsilon}G_b\right) - C_{2\varepsilon}\rho\frac{\varepsilon^2}{k} + S_\varepsilon \tag{4}$$

In equations (3)-(4): μ_i is the turbulent viscosity; G_k is the turbulent kinetic energy generation term caused by the average velocity gradient; G_b is the turbulent kinetic energy generation term caused by buoyancy effects; Y_M is the effect of compressible turbulent pulsation expansion on the total dissipation rate; $C_{1\varepsilon}$, $C_{2\varepsilon}$, $C_{3\varepsilon}$ is an empirical constant; σ_k, σ_ε are turbulent kinetic energy k and turbulent energy dissipation rate, respectively ε Corresponding Prandtl number; S_k, S_ε represents a user-defined source item.

2.2.2. Quantitative evaluation index of wind speed field uniformity

The velocity non-uniformity coefficient, the difference of wind speed sampling points and the average wind speed in the drying room are selected as the optimal scheme evaluation index of the uniformity of wind speed field in the drying room [18].

The velocity non-uniformity coefficient M is used to evaluate the uniformity of the velocity distribution in the drying room. The larger the M is, the more uneven the wind speed field is. The smaller the M, the better the uniformity of the wind speed field.

$$M = \frac{\sigma_V}{\overline{V}_a} \times 100\% \tag{5}$$

In equations (5): σ_V is the instantaneous speed; $\overline{V}_a$ is the overall mean of the velocity distribution.

The difference of wind speed sampling points: The data of the sampling points at the top and bottom of the drying area of the drying room are calculated by difference. In the comparative analysis, the uniformity of the wind speed field is better when the difference of the wind speed

sampling points is small.

$$\Delta V = V_1 - V_7 \tag{6}$$

In equations (6): ΔV is the calculation result of the difference of wind speed sampling points; V_1 is the wind speed data of sampling point P_1 ; V_7 is the wind speed data of sampling point P_7.

The average wind speed in the drying room: The value represents the strength of the airflow intensity. The strong airflow can have better circulation between the two sides of the airway and the sawn timber and remove the moisture in the sawn timber fully.

$$\bar{V}_a = \frac{\sum V_n}{n} \tag{7}$$

In equations (7): $\bar{V}_a$ is the overall mean of the velocity distribution ; V_n is the sampling point of each wind speed ; n is the number of sampling points, n=7.

2.2.3. Boundary conditions and Grid processing

The boundary condition is the conventional drying schedule, the temperature in the drying room is 60~110℃, the initial wind speed of the air inlet is set to 3m/s, and the air outlet is set to free air. The air flow in the drying room is regarded as incompressible turbulence, and the boundary layer is set to 5 layers. The standard k-ε model is used to construct the turbulence model of the wind speed field in the drying room, and the implicit solver and SIMPLE algorithm are selected for the velocity pressure coupling solution part. The grid model of the drying room The ICEM CFD software was used to mesh the simplified model under the loading condition of the hot air drying room (the total number of grids was 1857469), as shown in Figure 2.

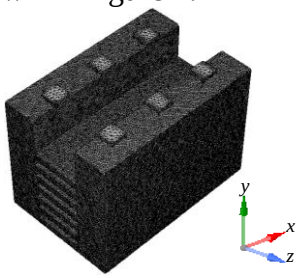

Figure 2: Grid results of the original structural model

2.2.4. Wind velocity field analysis of the original structure model

FLUENT is used to simulate the simplified model under the loading condition of the original structural model, and the wind speed field velocity distribution map of the key section is established at 1050 mm in the X-axis direction, as shown in Figure 3.

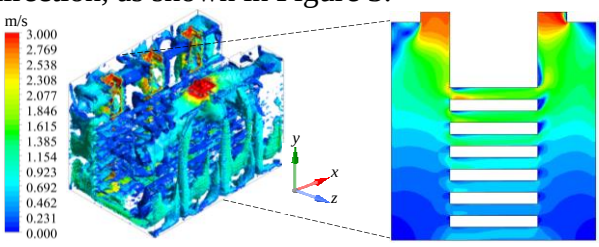

Figure 3: The wind velocity field velocity distribution of the key section of the original structure model

Through the analysis of the distribution of wind speed field in Figure 3, it can be seen that the three main causes of the uneven distribution of wind speed field in the drying room are as follows : A.There are low-speed turbulent areas in the left upper, left lower, right upper and right lower corners of the drying room wall ; B.The uniformity of wind speed in the air inlet and exhaust outlet is quite different from that in other areas of the drying room ; C.There is a large wind speed difference between the top and bottom of the sawn timber (dry zone).

2.2.5. Model reliability verification

The post-processing software CFD-POST was used to extract the simulated values in the numerical simulation results of the original structural model, and the data were compared with the measured values of the wind speed sampling points in the drying room (as shown in Table 1) to verify the reliability of the model.

Table 1: Comparison of measured values with simulated values and percentage deviations of wind speed sampling points

Data name	Wind speed sampling point /(m s^{-1})						
	P_1	P_2	P_3	P_4	P_5	P_6	P_7
Value of measured/(m s^{-1})	1.962	1.630	1.311	1.021	0.865	0.746	0.712
Value of simulation/(m s^{-1})	1.822	1.538	1.219	0.989	0.821	0.686	0.724
Percentage bias/%	7.14%	5.64%	7.02%	3.13%	5.09%	8.04%	1.69%

The maximum percentage deviation between the measured value and the simulated value in Table 1 is not more than 8.04%, and the change trend between the data is consistent, which can verify the accuracy and reliability of the numerical simulation results of the wind speed field of the original structural model. At the same time, the measured data of wind speed sampling points in Table 1 also reflect that there is indeed a problem of uneven distribution of wind speed field in the drying room and the wind speed difference is large.

2.3. Optimum structural design

In view of the main causes of the above three problems, a total of 8 schemes are proposed by using three structural optimization design methods: curved right-angle structure, adjustment of sawn timber spacing, and increase or decrease of the number of average wind plates. Among them, for the cause A, the right-angle structure surface method is used to form four schemes (A1.Change the upper left corner of the drying room to a curved surface structure. A2.Change the upper left corner and the lower left corner of the drying room into a curved structure. A3.Change the four corners of the drying room into a curved axisymmetric structure. A4.Change the drying room into an axisymmetric structure with vertex curved surface and bottom step curved surface).

For cause B, a combination of right-angle structure surface and saw spacing adjustment is used to form two schemes (B1.to adjust the saw spacing to a structure with narrow upper and wide lower. B2.Adjust the spacing of the sawn timber to the structure of upper width and lower narrow).

Aiming at the cause C, two schemes are formed by combining the right-angle structure curved surface with the adjustment of sawn timber spacing and the increase or decrease of the number of air-equalizing plates (C1. Add a curved air-equalizing plate to the left airway. C2.A flat plate and a curved plate were added to the left airway).

2.3.1. Analysis of wind speed field after structural optimization

Using the same numerical simulation method as the analysis of the wind speed field of the

original structure model, the numerical simulation of the eight structural optimization design schemes is carried out. The wind speed field velocity distribution of the key sections of each scheme is shown in Figure 4.

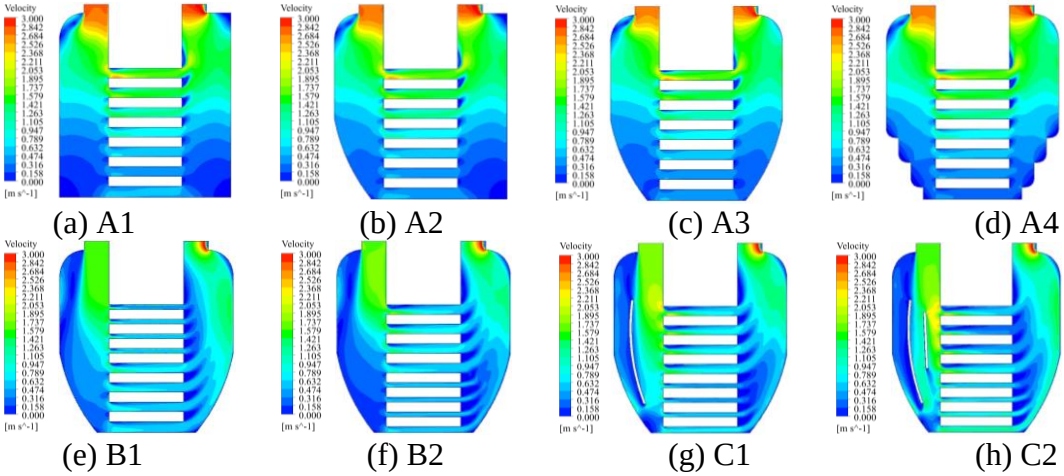

Figure 4: The wind velocity field velocity distribution diagram of the key section of the structural optimization design scheme

Because the energy exchange between the sawn timber and the hot air and the drying rate are directly affected by the wind speed value, in order to control the wind speed in the drying area within the ideal range of 1m/s to 3m/s [19], it is necessary to control the air inlet with different wind speeds (3m/s, 5m/s, 7m/s), and obtain a more uniform wind speed field by increasing the air flow speed. The wind speed sampling point data between the original structure model and the eight structural optimization schemes under different wind speed conditions are compared and analyzed, as shown in Figure 5.

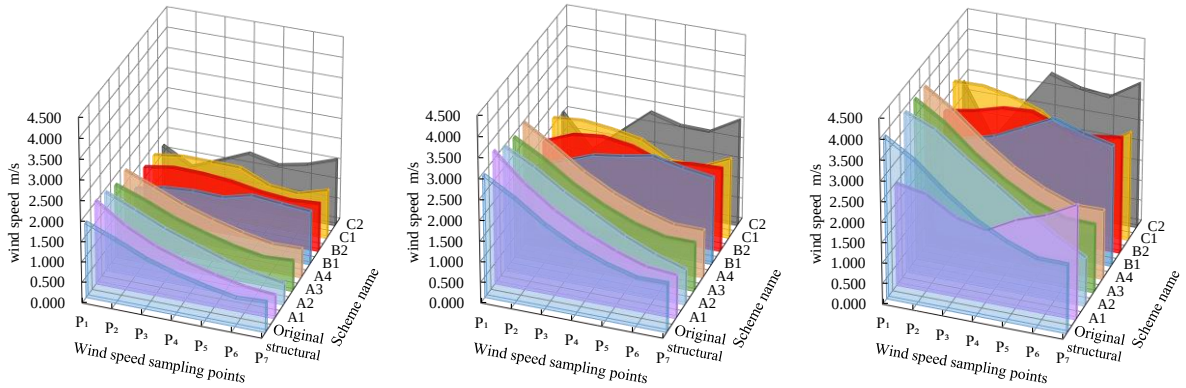

Figure 5: Comparison of wind speed sampling point data between different schemes under different wind speed conditions

In Figure 5a, when the wind speed is 3m/s, the wind speed sampling points of the original structural model and the scheme (A1, A2, A3, A4, C1, C2) are lower than the ideal range, and the ideal scheme accounts for 33.33%.

In Figure 5b, when the wind speed is 5m / s, the value of some wind speed sampling points in the scheme (A1, A2) is higher than the ideal range, and the ideal scheme accounts for 77.78%.

In Figure 5c, when the wind speed is 7m / s, the wind speed sampling points of the original structural model and the scheme (A2, A3, A4, B1, C1, C2) are higher than the ideal range, and the ideal scheme accounts for 22.22%.

In summary, when the inlet wind speed is 5m/s, the ideal scheme has the highest proportion, and it can be judged that the optimal wind speed configuration parameter of the inlet should be 5m/s. According to the analysis results of Figure 5, the distribution law of wind speed field in the drying room is that when the wind speed value of the air inlet increases, the value of the wind speed sampling point also increases synchronously, and vice versa. It can be judged that there is a positive correlation between the wind speed data of the air inlet and the wind speed sampling point data.

In order to obtain a more accurate optimal solution, the data comparison analysis and the empirical analysis of the effectiveness of the scheme will be further carried out. The velocity non-uniformity coefficient, wind speed sampling point difference and average wind speed in the drying room of each scheme under different wind speed conditions (3m/s, 5m/s, 7m/s) are calculated by using Eq.(5), Eq.(6) and Eq.(7). The relevant data are compared and analyzed, as shown in Table 2.

Table 2: Data comparison between structural optimization schemes under different wind speed conditions

Wind speed	Scheme name	Non-uniform velocity system *M*	Wind speed sampling point difference/(m s^{-1})	The average wind speed in the drying room/(m s^{-1})
3m/s	A1	0.459	1.483	1.094
	A2	0.437	1.420	1.115
	A3	0.353	1.061	1.114
	A4	0.368	1.141	1.114
	B1	0.079	-0.238	1.265
	B2	0.073	0.115	1.269
	C1	0.116	0.090	1.218
	C2	0.182	-0.436	1.249
5m/s	A1	0.408	2.188	1.846
	A2	0.410	2.180	1.839
	A3	0.349	1.762	1.833
	A4	0.359	1.833	1.834
	B1	0.110	-0.516	2.073
	B2	0.062	-0.110	2.069
	C1	0.112	0.238	1.972
	C2	0.189	-0.571	2.056
7m/s	A1	0.145	-0.282	2.257
	A2	0.372	2.735	2.556
	A3	0.324	2.267	2.549
	A4	0.322	2.239	2.548
	B1	0.104	-0.505	2.854
	B2	0.043	-0.108	2.871
	C1	0.126	0.496	2.748
	C2	0.205	-0.707	2.883

In Table 2, when the wind speed is 3m/s, scheme B2 has the smallest velocity non-uniformity coefficient and the largest average wind speed in the drying room among the eight structural optimization schemes, occupying two of the three quantitative evaluation indexes of wind speed field uniformity, so it is judged that scheme B2 is the optimal scheme under this working condition. When the wind speed is 5m/s, scheme B2 has the smallest speed non-uniformity coefficient, the smallest difference of wind speed sampling points, and the largest average wind speed in the drying

room among the eight structural optimization schemes, occupying three of the three quantitative evaluation indexes of wind speed field uniformity, so it is judged that scheme B2 is the optimal scheme under this working condition. When the wind speed is 7m/s, scheme B2 has the smallest speed non-uniformity coefficient, the smallest difference of wind speed sampling points and occupies two of the three quantitative evaluation indexes of wind speed field uniformity in the eight structural optimization schemes, so it is judged that scheme B2 is the optimal scheme under this working condition. In summary, Scheme B2 is the optimal scheme under different wind speed conditions (3m/s, 5m/s,7m/s), and when the inlet wind speed is 5m/s, Scheme B2 not only controls the wind speed in the dry zone within the ideal range of 1m/s to 3m/s, but also the quantitative evaluation index of wind speed field uniformity is also the optimal value.

The empirical analysis of the effectiveness of the scheme is further carried out, and the data before the optimization of the drying room structure (the original structure model) and after the optimization of the structure (the optimal scheme B2) are compared and analyzed, as shown in Table 3.

Table 3: Data comparison between the original structural model and the optimal scheme B2

Scheme name	Wind speed	Non-uniform velocity system *M*	Wind speed sampling point difference/(m s^{-1})	The average wind speed in the drying room/(m s^{-1})
Original structural model	3m/s	0.360	1.097	1.114
	5m/s	0.351	1.773	1.833
	7m/s	0.326	2.261	2.549
Optimal Scheme B2	3m/s	0.073	0.115	1.269
	5m/s	0.062	-0.110	2.069
	7m/s	0.043	-0.108	2.871

In Table 3, the optimal scheme B2 shows an effective improvement effect under different wind speed conditions (3m/s, 5m/s,7m/s). The velocity non-uniformity coefficient is the smallest, the wind speed sampling point difference is the smallest, and the average wind speed in the drying room is the largest.

2.3.2. Test result analysis

After comparing and analyzing the percentage deviation of the data (velocity non-uniformity coefficient, wind speed sampling point difference, average wind speed in the drying room) of the original structure model and the optimal scheme B2 at the inlet wind speed of 5m/s, it can be seen that the optimal scheme B2 is 82.34% lower than the velocity non-uniformity coefficient of the original structure model, the wind speed sampling point difference is reduced by 106.2%, and the average wind speed in the drying room is increased by 12.88%. The experimental results show that the optimal scheme B2 after structural optimization is lower than the low-speed turbulence area of the original structure model. The wind speed difference in the drying area is significantly reduced, and the uniformity of the wind speed in the drying room is effectively improved.

3. Conclusion

(1)Through the study of the distribution of wind speed field in the drying room under different wind speed conditions (3m/s,5m/s,7m/s), it is found that when the wind speed value of the air inlet increases, the value of the wind speed sampling point also increases synchronously, and vice versa. It can be seen that there is a positive correlation between the wind speed data of the air inlet and the wind speed sampling point data.

(2)The uniformity of wind speed field in the drying room can be effectively improved by combining the two design methods of curved right-angle structure and saw spacing adjustment. Among them, adjusting the spacing of sawn timber to the form of wide upper and narrow lower is more conducive to the better circulation of hot air flow between sawn timber, and the uniformity of wind speed field is also optimal.

(3)The optimal scheme B2 can effectively improve the uniformity of wind speed inside the drying room. The relevant design methods and research results can provide practical reference value for the structural optimization of similar hot air drying devices.

References

[1] Liu R., Dong J.X., Wang D., et al. Flow-field simulation and structural optimization of the chrysanthemum hot air drying room.[J].Journal of Machine design, 2021, 38(01):47-54.

[2] Elustondo D., et al.Advances in wood drying research and development.[J].Drying Technology, 2023,41(6):890-914.

[3] Shen Y.L., Wang Z., et al. Effect of Different Drying Methods on the Drying Characteristics of Plantation-Grown Pinus sylvestris var. mongolica.[J].Scientia Silvae Sinicae, 2020,56(11):151-158.

[4] MENG Z.X., QIAO J.B. Multi-Objective Optimization of Energy Consumption for Wood Drying Based on NSGA-II Algorithm [J]. China Forest Products Industry. 2023, 60(09):1-6.

[5] Fu Z.Y., Cai Y.C., Zhou Y.D., et al. Cuerent Staus and Prospects of Wood Drying Stresses Research.[J].Scientia Silvae Sinicae, 2021,57(9):160-167.

[6] Coban, S.O., et al. A review on computational fluid dynamics simulation methods for different convective drying applications.[J].Thermal Science, 2023,27(1B):825-842.

[7] Kadem, S., et al. Computational analysis of heat and mass transfer during microwave drying of timber.[J].Thermal Science, 2016,20(5):1447-1455.

[8] Chen Z.F., et al. Numerical simulation and experiment of four-way ventilation mixed flow drying section for rice.[J].Transactions of the Chinese Society of Agricultural Engineering (Transactions of the CSAE), 2022,38(24):237-247.

[9] Wang Z.W., et al. Optimal simulation design of structure and parameter in heat pump drying room.[J].Transactions of the Chinese Society for Agricultural Machinery, 2020,51(S):464-475.

[10] HUO P., et al. Optimization of Flow Field Uniformity in Drying Chamber Based on CFD.[J].China Ceramics, 2023,59(06):74-82.

[11] Li Q.H., et al. Analysis on the wind-speed field characteristics and the structure optimization of the power lithium battery's suspension oven.[J].Journal of Machine design, 2021,38(08):31-37.

[12] ZHANG X.Y., et al. Analysis and design study on the structural performance of new flow tube grate tooth seal for high altitude table.[J/OL].Journal of Aerospace Power,1-13[2024-03-28].https://doi.org/10.13224/j. cnki.jasp. 20230653.

[13] YU H.M., et al. Optimization Design and Performance Test of Multi-layer Tray Straw Tray Hot Air Assisted Microwave Drying Device.[J]. Transactions of the Chinese Society for Agricultural Machinery, 2023,54(11):397-411.

[14] Liu Y.H., et al. Optimal design and experimental verification of tilted tray air-impingement dryers.[J]. Transactions of the Chinese Society of Agricultural Engineering, 2022,38(05):269-278.

[15] WU M., et al. Design and Experiment of Infrared-hot Air Combined Dryer Based on Temperature and Humidity Control.[J]. Transactions of the Chinese Society for Agricultural Machinery, 2020, 51(S1):483-492.

[16] Jiang D.L., et al. Desing and Performance Verification of Infrared Combined Hot Air Drying Device.[J]. Transactions of the Chinese Society for Agricultural Machinery, 2022,53(12):411-420.

[17] Tang H.T., et al. Aerodynamic Characteristics Analysis of Curve Overtaking Based on CFD.[J].Journal of Engineering Mechanics and Machinery, 2023,8(4):85-96.

[18] Zhu Y.F., et al. Influence of improved structure of drying kiln on the uniformity of wind velocity flow field.[J].Transactions of the Chinese Society of Agricultural Engineering, 2021,37(24):327-337.

[19] Ding Y., et al. Simulation and optimization of wind field inside veneers solar drying kiln. [J].Journal of Northeast Forestry University, 2021,49(2):101-106.